Low-Dimensional ReS2/C Composite as Effective Hydrodesulfurization Catalyst

Article *in* Catalysts · December 2017

DOI: 10.3390/catal7120377

8 authors, including:

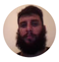

Juan Antonio Aliaga
Universidad Tecnológica Metropolitana
20 PUBLICATIONS **62** CITATIONS
SEE PROFILE

T. A. Zepeda
Universidad Nacional Autónoma de México
68 PUBLICATIONS **1,100** CITATIONS
SEE PROFILE

Juan-Francisco Araya
University of Concepción
51 PUBLICATIONS **221** CITATIONS
SEE PROFILE

Eglantina Benavente
Universidad Tecnológica Metropolitana
73 PUBLICATIONS **1,182** CITATIONS
SEE PROFILE

catalysts

MDPI

Communication

Low-Dimensional ReS_2/C Composite as Effective Hydrodesulfurization Catalyst

Juan Antonio Aliaga [1,2,*], Trino Zepeda [3], Juan Francisco Araya [4], Francisco Paraguay-Delgado [5], Eglantina Benavente [2,6], Gabriel Alonso-Núñez [3], Sergio Fuentes [3] and Guillermo González [6,7]

[1] Programa Institucional de Fomento a la Investigación, Desarrollo e Innovación (PIDi) Universidad Tecnológica Metropolitana, Ignacio Valdivieso 2409, San Joaquín 8940577, Santiago, Chile
[2] Departamento de Química, Universidad Tecnológica Metropolitana, Las Palmeras 3360, Ñuñoa, Santiago, Chile; ebenaven@utem.cl
[3] Centro de Nanociencia y Nanotecnología, Universidad Nacional Autónoma de México, Ensenada 22860, Baja California, Mexico; trino@cnyn.unam.mx (T.Z.); galonso@cnyn.unam.mx (G.A.-N.); fuentes@cnyn.unam.mx (S.F.)
[4] Centro de Investigaciones Costeras de la Universidad de Atacama, Universidad de Atacama, Copayapu 485, Copiapó, Chile; juan.araya@uda.cl
[5] Departamento de Física de Materiales, Centro de Investigación Materiales Avanzados S.C., Chihuahua 31136, Mexico; francisco.paraguay@cimav.edu.mx
[6] Center for the Development of Nanoscience and Nanotechnology, CEDENNA, Av. Ecuador 3493, Santiago, Chile; ggonzale@uchile.cl
[7] Departamento de Química, Facultad de Ciencias, Universidad de Chile, Las Palmeras 3425, Santiago, Chile
* Correspondence: jaliaga@utem.cl

Received: 30 October 2017; Accepted: 29 November 2017; Published: 5 December 2017

Abstract: Single-layer, ultrasmall ReS_2 nanoplates embedded in amorphous carbon were synthesized from a hydrothermal treatment involving ammonium perrhenate, thiourea, tetraoctylammonium bromide, and further annealing. The rhenium disulfide, obtained as a low dimensional carbon composite (ReS_2/C), was tested in the hydrodesulfurization of light hydrocarbons, using 3-methylthiophene as the model molecule, and showed enhanced catalytic activity in comparison with a sulfide CoMo/γ-Al_2O_3 catalyst. The ReS_2/C composite was characterized by X-ray diffraction (XRD), Raman spectroscopy, N_2 adsorption–desorption isotherms, scanning electron microscopy (SEM), scanning transmission electron microscopy (STEM), energy-dispersive X-ray spectroscopy (EDS), and X-ray photoelectron spectroscopy (XPS). The improved catalytic performance of this ReS_2/C composite may be ascribed to the presence of a non-stoichiometric sulfur species (ReS_{2-x}), the absence of stacking along the *c*-axis, and the ultra-small basal planes, which offer a higher proportion of structural sulfur defects at the edge of the layers, known as a critical parameter for hydrodesulfurization catalytic processes.

Keywords: rhenium disulfide; hidrodesulfurization; light S-hydrocarbons; thiophene; 3-methylthiophene; solvothermal synthesis; single layer

1. Introduction

Rhenium disulfide (ReS_2) presents a two-dimensional (2D) layered structure similar to those of other Transition Metal Dichalcogenides (TMDC), where the atoms within layers are bonded by covalent interactions; the layers in these TMDC are stacked, and held together by van der Waals forces, forming a sandwich-like structure analogous to graphite [1,2]. The electronic and vibrational behavior of ReS_2 in bulk resembles that of a particular single-layer TMDC species, which can be explained as a Peierls distortion of the ReS_2 structure [3]. The anisotropic and electronic characteristics of this layered TMDC have also shown promising applications in many fields, including its use as an effective hydrotreating catalyst [4,5] and electrocatalyst [6,7], as well as in gas sensing [8,9], batteries [10–12], and photodetectors [13,14]. The synthesis of ReS_2 has received special attention due to its recently discovered distinctive properties, which may derive from its electronic structure [15]. However, most of the syntheses are directed to the production of single crystalline layers, or few-layer thin crystals for electronic applications [16]. These ordered compounds have been successfully obtained by chemical vapour deposition (CVD) [17,18], by physical vapour desposition (PVD) [19], and by microwave-induced plasma methods [20]. In contrast, TMDC catalysts require products with disordered and defect-rich structures, as well as high surface areas and poorly stacked layers [21]. Solvothermal methods are fruitful for this purpose; using these methods, the synthesis of defect-rich structures can be achieved with the assistance of organic moieties, voluminous organic cations [22], ionic liquids [23] and by the use of carbonaceous sulfidizing agents (thiourea, thioacetamide, L-cysteine). Thiourea, in particular, has also been used to stabilize defect-rich and ultrathin MoS_2 nanosheets [24].

Solvothermal methods have been scarcely applied to the synthesis of ReS_2 composites. ReS_2 composites are materials with potential applications in catalysis processes such as hydrodesulfurization (HDS) and hydrogen evolution (HER) reactions, due to the synergy between the electronic nature and the intrinsically low stacking of the ReS_2 layers, and due to the morphologies of the products derived from the carbonaceous scaffolding [5,6,12]. In this paper, we explore a new approach to the synthesis of low-dimensional ReS_2 layers—namely, by the hydrothermal sulfurization of a rhenium precursor (NH_4ReO_4), assisted by tetraoctylammonium bromide, followed by annealing at 400 °C. This product was tested in the hydrodesulfurization of 3-methylthiophene (3MT), showing a higher catalytic activity in comparison with a sulfided $CoMo/\gamma\text{-}Al_2O_3$. The present synthesis—besides allowing the obtainment of a ReS_2/C composite with peculiar structure and textural properties—may be applied to the preparation of a new generation of ReS_2 composite catalysts.

2. Results

2.1. Characterization of the Catalyst

2.1.1. X-ray Diffraction and Raman Spectroscopy Analysis

The crystallinity and phase purity of the composite were analyzed by XRD and Raman spectroscopy. Figure 1a shows a XRD diffraction pattern for the ReS_2/C sample annealed at 400 °C. The diffractogram only shows weak broad peaks at about $2\theta = 33°$ and $59°$, corresponding to the (200) and (220) reflections of triclinic ReS_2 [2]. The absence of the (002) diffraction peak at $2\theta = 14.5°$ indicates an extremely low stacking along the (001) direction, pointing to the presence of crystallographically-independent ReS_2 layers [25]. The absence of the (002) reflection has been reported for MoS_2 and WS_2 layers with no preferential orientation and random arrangement [26,27]. The Raman spectrum showed in the Figure 1b indicates the characteristic Raman modes (labeled III to V) for ReS_2 [3,28]. The signal located ~157 cm^{-1} corresponds to the overlap of Eg-like (III and IV) vibrations, and the peak at ~210 cm^{-1} resulted from the Ag-like (V) vibrational mode. The overlap of the Eg-like vibrations may have arisen from the random arrangement and poorly crystalline phase of the ReS_2 in the composite. Also, the formation of amorphous carbon, expected to be formed by the decomposition of the alkylammonium salt [29], was corroborated by the presence of the D and G carbon bands at 1362 and 1578 cm^{-1} [26].

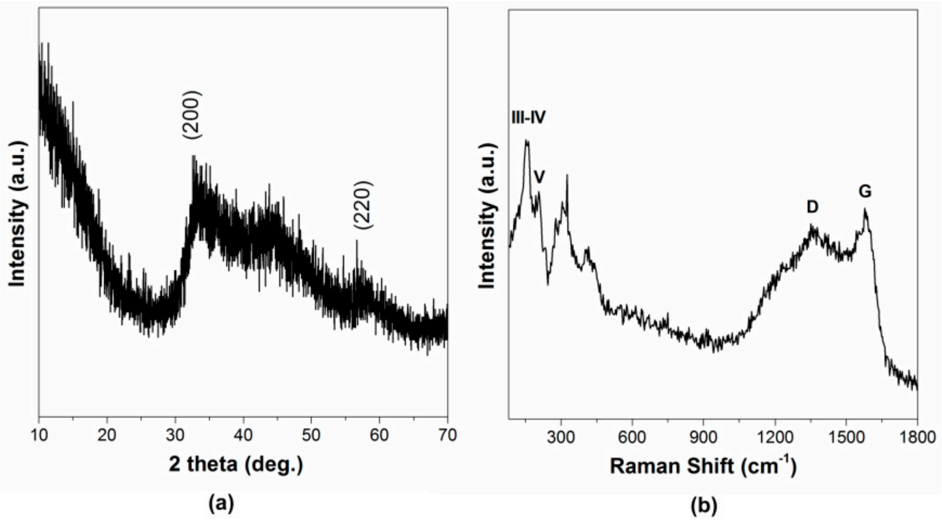

Figure 1. (**a**) X-ray Diffraction (XRD) pattern and (**b**) Raman spectra of ReS_2/C nanolayers annealed at 400 °C for 1 h under argon atmosphere.

2.1.2. Surface Area Analysis

Figure 2 shows the nitrogen adsorption–desorption isotherm for the ReS_2/C composite. The isotherms have a shape type IV, associated with large size mesoporous types, and the H3 hysteresis loop indicated the presence of a slit nanopore [30,31]. This sample had a specific Brunauer Emmer Teller (BET) surface area of 87 $m^2\ g^{-1}$. The desorption, Barrett−Joyner−Halenda (BJH) pore size distribution is shown in Figure S2, which indicates a large number of pores circa 38.39 Å, with a total pore volume of 0.095 cm^3/g. These results are comparable to those of other TMDC materials composed by highly destacked layers [32], as well as to those of the ReS_2 obtained by thermal decomposition of tetraalkylammonium tetratioperrhenate [33]. In this regard, it is known that the carbonaceous matter derived from the decomposition of tetraoctylammonium bromide or other carbonaceous salts changes the textural properties of metal sulfides, increasing their surface area [34].

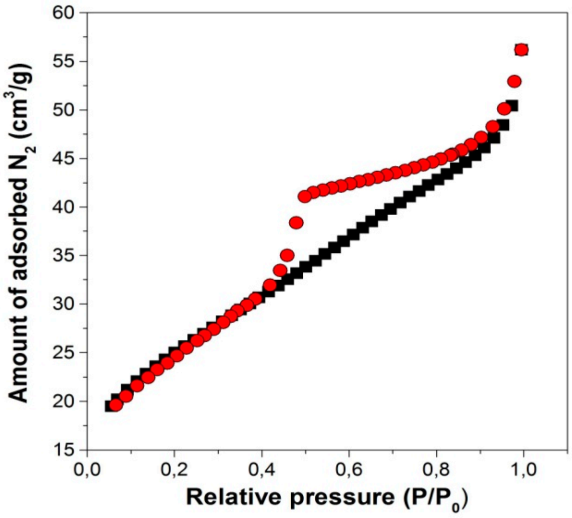

Figure 2. N_2 adsorption–desorption isotherm of ReS_2/C nanolayers. Black squares indicate adsorption and the red circles desorption.

2.1.3. X-ray Photoelectron and Energy-Dispersive X-ray Spectroscopy

The chemical state of the ReS_2/C composite was investigated by X-ray photoelectron spectroscopy (XPS). Figure 3a,b shows XPS spectra of ReS_2 concerning core level electrons of rhenium (Re 4f) and sulfur (S2p), respectively. Figure 3a shows two Re 4f peaks at 41.4 eV and 43.8 eV, corresponding to the core levels $4f_{7/2}$ and $4f_{5/2}$ respectively for Re^{+4}. Figure 3b shows two S2p characteristic peaks located at 161.8 eV and 163.0 eV, ascribed respectively to the core levels $2p_{3/2}$ and $2p_{1/2}$ of S^{-2} [28,35]. Also, the S/Re atomic ratio obtained by XPS was about 1.8, indicating the formation of sulfur-deficient ReS_{2-x} layers, which is consistent with the energy-dispersive X-ray spectroscopy (EDS) spectrum analysis (Figure S1). The elemental composition of the ReS_2/C sample was determined by EDS and is listed in the Table S1, where it can be observed that the composite contained Re, S, C and O. The calculated S/Re and C/Re atomic ratios were 1.79 and 3.62, respectively. The carbon element was provided by the decomposition of the tetraoctylammonium cation during the hydrothermal process and further annealing. The oxygen element observed in the analysis was from the amorphous carbon, which was not reduced completely during the annealing at 400 °C.

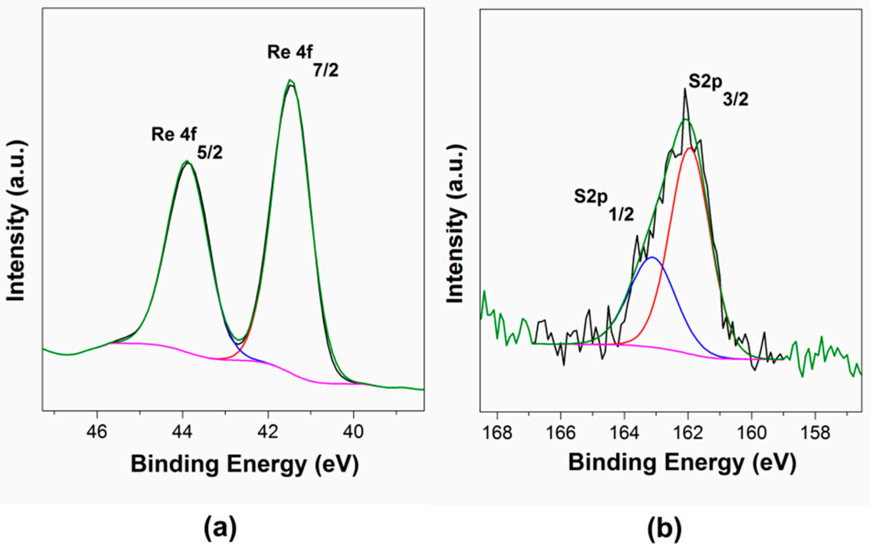

Figure 3. X-ray photoelectron spectroscopy (XPS) spectra of (**a**) Re 4f and (**b**) S2p core levels of the ReS_2/C composite.

2.1.4. Scanning Transmission Electron Microscopy Analysis

The morphological and microstructure features of the ReS_2/C sample annealed at 400 °C were investigated by scanning transmission electron microscopy (STEM). The high-angle annular dark-field (HAADF) and bright-field scanning transmission electron microscopy (BF-STEM) images of the material are shown in Figure 4a,b, respectively. Figure 4a gives a general view of a grain, consisting of large fluffy zones; a magnification of one of these fluffy arrangements (Figure 4b) shows a particle-rich zone, containing randomly-orientated ReS_2 layers. The amorphous carbon dispersant matrix can be detected in Figure 4c, where the bright atom contrast arises from the ReS_2 layers, while carbon atoms show lower contrast. The small average lateral sizes (4.22 ± 1.39 nm) and low stacking (1–2 stacked layers) of the ReS_2 layers observed in the present product are similar to those in ReS_2 composites obtained by the sulfidization of tetraalkylammonium perrhenate salts [25]. The small and randomly-orientated ReS_2 layers shown in the STEM images (Figure 4c,d), correspond with the absence of the (002) plane, as well as with the XRD broadened reflection described above.

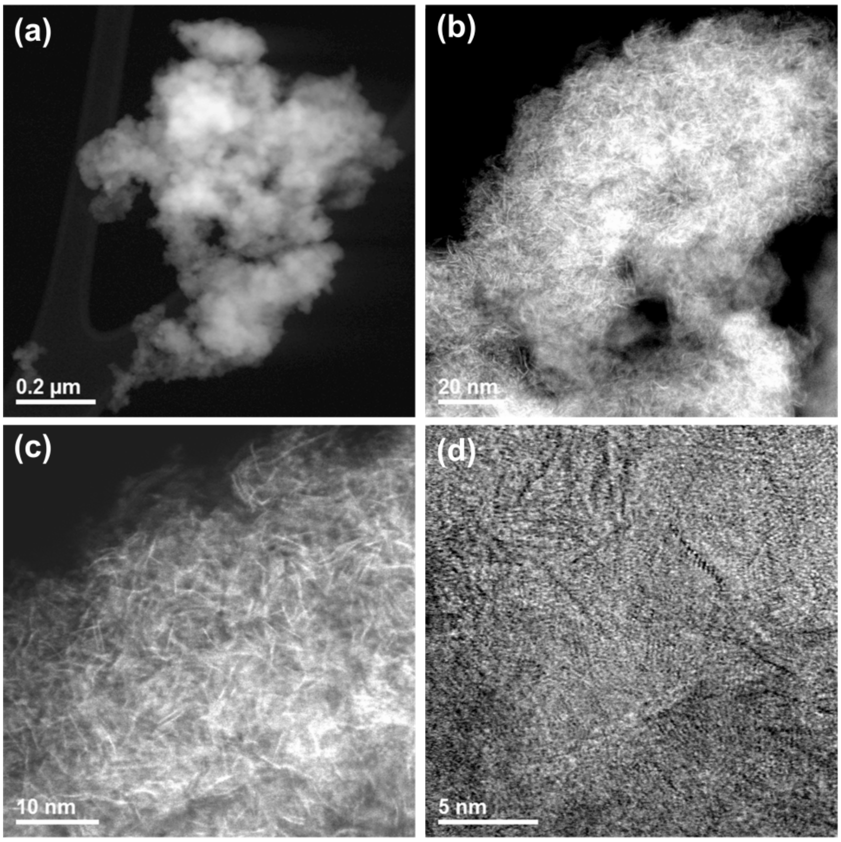

Figure 4. (**a**–**c**) High-angle annular dark-field (HAADF) scanning transmission electron microscopy (STEM) and (**d**) high-resolution transmission electron microscopy (HRTEM) images of ReS_2/C composite.

The formation of the ReS_2/C composite with special textural properties can be explained considering the nature of the main source of carbonaceous matter, which is the bulky octylammonium salt. Indeed, the hydrothermal sulfidization of NH_4ReO_4 with thiourea, but without further annealing and the assistance of alkylammonium salt, leads to the formation of few-layered ReS_2 nanosheets [11,12]. The ultra-small-sized basal plane, as well as the absence of stacking of the synthesized ReS_2 layers, can be rationalized, considering the presence of carbonaceous matter which hinders the growing and ordering of the inorganic layers (edge to edge attachment and face to face stacking) during formation of the ReS_2/C composite [25].

2.2. Hydrodesulfurization Activity

The ReS_2/C composite catalyst was evaluated in the hydrodesulfurization (HDS) of 3-methyl-thiophene at 280, 300, 320 and 340 °C under atmospheric pressure, using a sulfided $CoMo/\gamma\text{-}Al_2O_3$ catalyst as reference. The reaction rate ($mol_{3\text{-}MT}\ g^{-1}\ Cat{\cdot}s^{-1}$) was considered as an activity parameter. The HDS reaction rates were measured at different temperatures for both the ReS_2/C composite and the reference catalyst, as were their respective apparent activation energies, which are listed in Table 1. At the lowest temperature measured, 280 °C, both catalysts show a similar catalytic activity at 35–37 ($10^{-8}\ mol_{3\text{-}MT}\ g^{-1}{\cdot}Cat{\cdot}s^{-1}$). At higher reaction temperatures, the catalytic performance of ReS_2/C is notably superior; in fact, at 340 °C the ReS_2 composite was 31% more active than the reference catalyst. In order to compare the performance of both evaluated catalysts, the apparent activation energies (Ea) were estimated for each sample through Arrhenius plots. The Ea calculated were 94 and 75 kJ mol^{-1} respectively for the ReS_2/C and for the sulfided $CoMo/\gamma\text{-}Al_2O_3$ catalyst; these results show the same paradoxical behavior for recently described ReS_2 catalysts [5].

Table 1. Reaction rates and apparent activation energies (Ea) for the catalysts evaluated in a flow reactor and calculated under kinetic control in steady-state conditions (conversions between 15% and 20%) and atmospheric pressure conditions at 280, 300, 320 and 340 °C.

Sample	**Rate (10^{-8} mol$_{3\text{-MT}}$ g^{-1}·Cat·s^{-1})**				**Ea (kJ mol^{-1})**
	280 °C	**300 °C**	**320 °C**	**340 °C**	
ReS_2/C	35	74	148	251	94
CoMo/Al_2O_3	38	67	121	191	75

In order to understand the differences between the Re- and Mo-based catalysts, the selectivity data was analyzed. The reaction products identified were 3-methyl-tetrahydrothiophene (3MTHT), 2-methyl-1,3-butadiene (Isoprene), 3-methyl-1-butene (3M1B), 2-methyl-1-butene (2M1B), 2-methyl-2-butene (2M2B), 2-methyl-butane (2MB), 1-pentene (1P) and a mixture (*cis*- and *trans*-) of 2-pentene (2P). The reaction path network proposed for the present reaction is shown in Figure 5. From that figure, it can be noted that the HDS reaction proceeds via pathways of hydrogenation (HYD) and direct desulfurization (DDS). The HYD pathway was proposed due to the presence of 3MTHT; this product can be transformed during the reaction process into isoprene and/or to the completely hydrogenate product 2MB. The DDS path leads to the formation of isoprene and its subsequent transformation (isoprene conversion) to an olefin mixture (3M1B, 2M1B, and 2M2B); we call this last stage the first hydrogenation pathway. Even when there was a presence of mixed olefin compounds (3M1B, 2M1B, and 2M2B) in the pathway, it was also possible to obtain the 2MB compound through a second hydrogenation. Furthermore, pentenes (1P and a mixture of *cis*- and *trans*-2P), were formed due to the isomerization of the mixed olefin compounds.

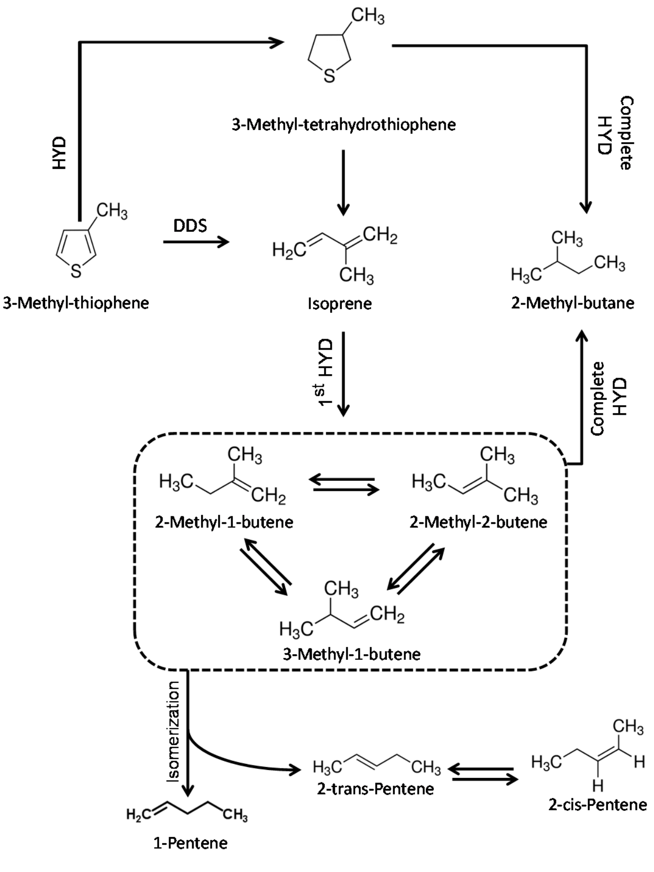

Figure 5. Reaction path network for the 3-methyl-thiophene hydrodesulfurization. DDS: desulfurization; HYD: hydrogenation.

The selectivity data taken at a 3MT conversion of 20–25% for ReS_2/C and the reference catalyst are shown in Figure 6. It can be noted that the principal product observed over both catalysts was the mixed olefins compounds (3M1B, 2M1B, and 2M2B), which were obtained via the first hydrogenation pathway from isoprene transformation. The formation of olefin compounds was higher over the ReS_2/C than over the molybdenum reference catalyst. One can even notice an important change in the fraction of olefin formation with the temperature increase (from 80 up to 89%). Conversely, the formation of mixed olefin over the reference sulfided CoMo/γ-Al_2O_3 catalyst remains close to 75%, being largely independent of the temperature change. The highest fraction of isoprene and 3MTHT selectivity (DDS and HYD pathways, respectively) were observed over the CoMo-based catalyst. In both samples (Re- and CoMo-based catalysts), the fraction of these compounds formed slightly decreased as the temperature increased, and their decrement was similar in both samples. This was expected to occur, because the thermodynamic stability of these products adsorbed on the catalyst surface should be lower at higher temperatures. The selectivity of the products obtained by isomerization steps (mix of pentenes) significantly decreased with a rise of temperature in both catalysts. In addition, the selectivity of the products of the complete hydrogenation step (2MB) decreased over the ReS_2/C catalyst and increased in the reference catalyst as the temperature increased.

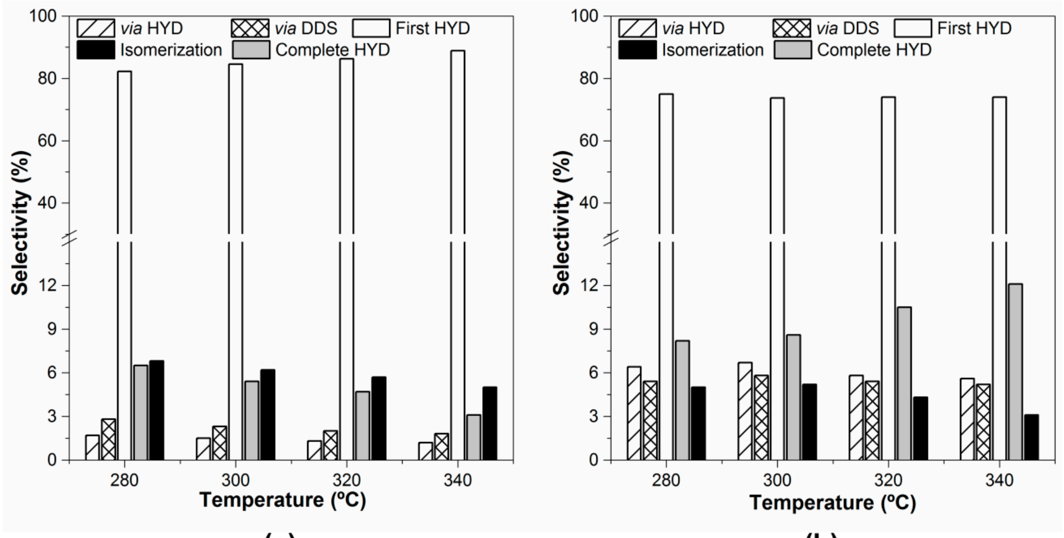

(a) (b)

Figure 6. Selectivity taken to 20–25% of 3-methyl-thiophene conversion in (**a**) ReS_2/C composite and (**b**) reference sulfided CoMo/γ-Al_2O_3.

In order to understand the isomerization and hydrogenation abilities of both catalysts, the ratios of selectivity of Olefin/2MB and Olefin/Isomerization versus the reaction temperature were calculated from the same 3MT conversion (20–25%) (Figure 7). There was a notable difference between the Olefin/2MB ratio for both catalysts, as can be seen in Figure 7a, where one can see a marked increase of the ReS_2/C selectivity to olefin formation as the reaction temperature increases. The opposite was observed for the CoMo-based catalyst. In the case of the relationship between olefin/isomerization ratio and the temperature reaction, a similar trend can be seen for Re- and CoMo-based catalysts (Figure 7b). The comparatively higher catalytic performance of the Re-based catalyst in the hydrodesulfurization of 3MT, in comparison to that of a supported Mo catalyst promoted by cobalt (CoMo/γ-Al_2O_3), may have arisen from the presence of a non-stoichiometric sulfur species (ReS_{2-x}) in the synthesized composite, in the absence of stacking along the *c*-axis, and in the ultra-small basal planes, which offer a higher proportion of structural sulfur defects at the edge of the layers. These sulfur defects are critical for hydrodesulfurization catalytic processes. The high yield of olefins obtained with the Re-based catalyst, in comparison with the reference catalyst, may have arisen from the presence of more than one active site, involving HYD and DDS reactions, according to the rim-edge catalytic model [36]. These results indicate that the low hydrogenation ability of the ReS_2 catalyst, in comparison with the promoted CoMo catalyst, as well as the comparatively high olefin formation produced by the ReS_2/C composite catalyst, may favor the production of gasolines with a greater octane number.

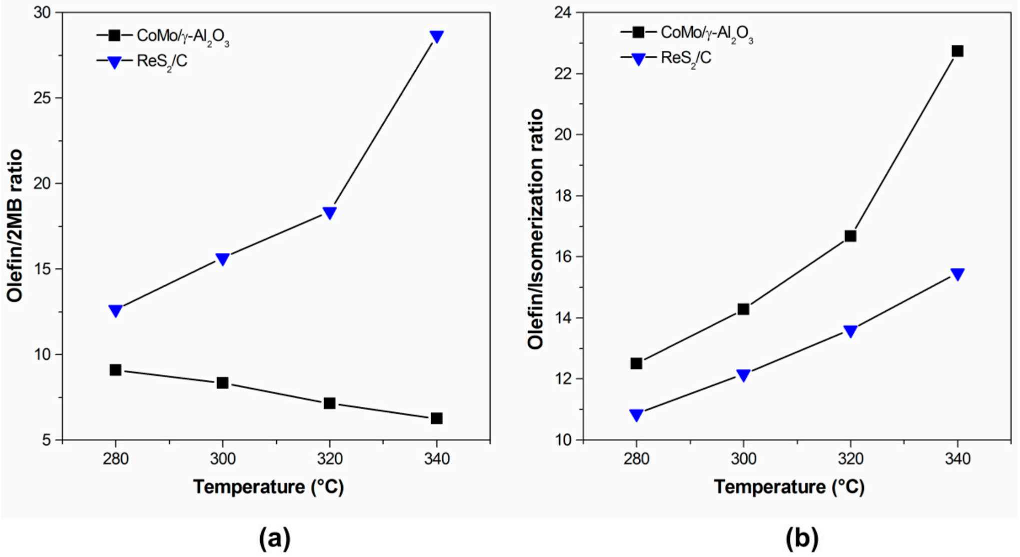

Figure 7. (**a**) Olefin/isomerization and (**b**) Olefin/2MB ratios versus the reaction temperature.

3. Materials and Methods

3.1. Preparation of Catalyst

An amount of 0.3 mmol of analytically pure NH_4ReO_4, 0.15 mmol of tetraoctylammonium bromide (TOA), 0.9 mmol of thiourea, and 2 mL of deionized water were put into a Teflon-lined 3 mL stainless steel autoclave and heated in an electrical oven for 48 h at 180 °C. The reactor was then cooled down naturally, giving a black powder. The powder was further annealed, by heating it at about 20 °C min^{-1} up to 400 °C under an Ar flow rate of about 20 mL min^{-1} in a conventional tube furnace, where it was maintained at this temperature for another hour.

3.2. Characterization and Catalytic Activity Measurements

X-ray powder diffraction (XRD) patterns were obtained by a Philips X'pert MPD powder diffractometer operating at 30 mA and 40 kV, using CuKα radiation (k = 1.54 Å). Raman spectra were recorded with a Witec Alpha 300 System instrument (Ulm, Germany) equipped with a 514 nm laser line. Scanning electron microscopy (SEM) photographs were taken in a JEOL JIB 4500 (Tokyo, Japan) electron microscope operated at 15 kV. Scanning transmission electron microscopy (STEM) and energy-dispersion X-ray (EDS) spectroscopy were conducted using a JEOL 2000FS (Peabody, MA, USA) operating at 200 kV. X-ray Photoelectron Spectra (XPS) were carried out in a SPECS–PHOIBOS-150 WAL hemispherical electron analyzer and a μ-FOCUS 500 X-ray source (Berlin, Germany), the sample charging correction was done against adventitious carbon (C 1s 284.8 eV). The specific surface area was measured by a Quantasorb system Model QS-17 Quantachrome Instrument (Boyton Beach, FL, USA).

The 3-methyl-thiophene (3MT) hydrodesulfurization (HDS) reaction was carried out in vapor phase using a homemade, fixed-bed micro flow reactor (15 mm ID), housed in a furnace. The reaction was evaluated using the ReS_2/C synthesized catalyst, with the sulfided CoMo/γ-Al_2O_3 commercial catalyst (KF 757 STARS, Akzo Nobel, Amsterdam, The Netherlands) as a reference. The reactor was loaded with 100 mg of catalyst diluted with 1 g of SiC. Prior to the catalytic test, the sample was dried under a N_2 flow of 50 mL min^{-1} at 150 °C for 30 min, to eliminate any moisture which could be adsorbed on the catalyst surface. The reaction was carried out at a series of different temperatures—280, 300, 320 and 340 °C—under hydrogen atmosphere at normal pressure. Meanwhile, the hydrogen saturation with 3MT was obtained by bubbling a H_2 flow (70 mL min^{-1}) through a saturator containing liquid 3MT at 20 °C. Steady-state conditions were reached after one hour of a time-on-stream reaction. Reaction products were analyzed by on-line gas chromatography (Agilent-7820, FID, DB-1 column of 30 m, Santa Clara, CA, USA).

4. Conclusions

In summary, for the first time, crystallographically-independent, ultra-small ReS_2 layers embedded in amorphous carbon were successfully obtained through a mild-energy hydrothermal route, using thiourea, tetraoctylammonium bromide, and ammonium perrhenate with further annealing. The structural characterization shows that these ReS_2 layers are the smallest ones obtained through a low temperature synthesis, with very small average lateral sizes (4.22 ± 1.39 nm) and a low stacking (1–2 stacked layers). The specific surface area of the ReS_2/C composite (87 m^2/g) was also the highest found for a ReS_2 composite. The catalytic performance of this compound in the hydrodesulfurization of 3MT was comparatively better than that of a commercial sulfided CoMo/γ-Al_2O_3 catalyst, under the same conditions. The improved catalytic performance of this novel composite may be ascribed to the presence of a non-stoichiometric sulfur species (ReS_{2-x}), the absence of stacking along the *c*-axis, and in the ultra-small basal planes, which offer a higher proportion of structural sulfur defects at the edge of the layers, which are known to be a critical parameter for hydrodesulfurization catalytic processes. The synthesis strategy herein reported—besides allowing for the obtaining a ReS_2/C composite with peculiar structure and textural properties, which are highly promising as material for hydrodesulfurization processes—may be expandable to the preparation of a new generation of rhenium sulfide-based catalysts.

Supplementary Materials: The following are available online at www.mdpi.com/2073-4344/7/12/377/s1, Figure S1: EDS of ReS_2/C nanolayers annealed at 400 °C for 1 h under argon atmosphere. Figure S2: Pore size distribution of the ReS_2/C nanolayers annealed at 400 °C. Table S1: Elemental composition of the ReS_2/C nanolayers annealed at 400 °C.

Acknowledgments: The authors thank CONICYT (FONDECYT Grant 1171803 and post-doctoral project 3170761), CEDENNA, CONACYT (174689, 152012 and 117373), PAPIIT (IN104714). The authors are grateful to E. Flores, E. Aparicio, D. Dominguez, M. Mack and I. Gradilla for their technical assistances. We are also indebted to the anonymous reviewers for their helpful corrections, suggestions, and comments, which improved the manuscript.

Author Contributions: Juan Aliaga, Trino Zepeda, Gabriel Alonso-Núñez and Guillermo González conceived and designed the experiments; Trino Zepeda, Juan Antonio Aliaga and Francisco Paraguay-Delgado performed the experiments; Juan Antonio Aliaga, Trino Zepeda, Juan Francisco Araya, Francisco Paraguay-Delgado, Eglantina Benavente, and Sergio Fuentes analysed the data and discussed results; Juan Antonio Aliaga, Juan Francisco Araya and Trino Zepeda wrote the manuscript.

Conflicts of Interest: The authors declare no conflict of interest.

References

1. Wildervanck, J.; Jellinek, F. The dichalcogenides of technetium and rhenium. *J. Less Common Met.* **1971**, *24*, 73–81. [CrossRef]
2. Lamfers, H.J.; Meetsma, A.; Wiegers, G.; De Boer, J. The crystal structure of some rhenium and technetium dichalcogenides. *J. Alloy Compd.* **1996**, *241*, 34–39. [CrossRef]
3. Tongay, S.; Sahin, H.; Ko, C.; Luce, A.; Fan, W.; Liu, K.; Zhou, J.; Huang, Y.-S.; Ho, C.-H.; Yan, J.; et al. Monolayer behaviour in bulk ReS_2 due to electronic and vibrational decoupling. *Nat. Commun.* **2014**, *5*, 3252–3257. [CrossRef] [PubMed]
4. Ho, T.; Shen, Q.; McConnachie, J.; Kliewer, C. Kinetic characterization of unsupported ReS_2 as hydroprocessing catalyst. *J. Catal.* **2010**, *276*, 114–122. [CrossRef]

5. Aliaga, J.; Zepeda, T.; Pawelec, B.; Araya, J.; Antúnez-García, J.; Farías, M.; Fuentes, S.; Galván, D.; Alonso-Núñez, G.; González, G. Microspherical ReS_2 as a High-Performance Hydrodesulfurization Catalyst. *Catal. Lett.* **2017**, *147*, 1243–1251. [CrossRef]
6. Wang, L.; Sofer, Z.; Luxa, J.; Sedmidubsky, D.; Ambrosi, A.; Pumera, M. Layered rhenium sulfide on free-standing three-dimensional electrodes is highly catalytic for the hydrogen evolution reaction: Experimental and theoretical study. *Electrochem. Commun.* **2016**, *63*, 39–43. [CrossRef]
7. Gao, J.; Li, L.; Tan, J.W.; Sun, H.; Li, B.C.; Idrobo, J.C.; Singh, C.V.; Lu, T.M.; Koratkar, N. Vertically Oriented Arrays of ReS_2 Nanosheets for Electrochemical Energy Storage and Electrocatalysis. *Nano Lett.* **2016**, *16*, 3780–3787. [CrossRef] [PubMed]
8. Yang, A.; Gao, J.; Li, B.; Tan, J.; Xiang, Y.; Gupta, T.; Li, L.; Suresh, S.; Idrobo, J.C.; Lu, T.-M. Humidity sensing using vertically oriented arrays of ReS_2 nanosheets deposited on an interdigitated gold electrode. *2D Mater.* **2016**, *3*, 1–7. [CrossRef]
9. Yang, S.; Kang, J.; Yue, Q.; Coey, J.; Jiang, C. Defect-Modulated Transistors and Gas-Enhanced Photodetectors on ReS_2 Nanosheets. *Adv. Mater. Interfaces.* **2016**, *3*, 1–5. [CrossRef]
10. Zhang, Q.; Tan, S.; Mendes, R.G.; Sun, Z.; Chen, Y.; Kong, X.; Xue, Y.; Rümmeli, M.H.; Wu, X.; Chen, S. Extremely Weak van der Waals Coupling in Vertical ReS_2 Nanowalls for High-Current-Density Lithium-Ion Batteries. *Adv. Mater.* **2016**, *28*, 2616–2623. [CrossRef] [PubMed]
11. Qi, F.; Chen, Y.; Zheng, B.; He, J.; Li, Q.; Wang, X.; Yu, B.; Lin, J.; Zhou, J.; Li, P. 3D chrysanthemum-like ReS_2 microspheres composed of curly few-layered nanosheets with enhanced electrochemical properties for lithium-ion batteries. *J. Mater. Sci.* **2017**, *52*, 3622–3629. [CrossRef]
12. Qi, F.; He, J.; Chen, Y.; Zheng, B.; Li, Q.; Wang, X.; Yu, B.; Lin, J.; Zhou, J.; Li, P. Few-layered ReS_2 nanosheets grown on carbon nanotubes: A highly efficient anode for high-performance lithium-ion batteries. *Chem. Eng. J.* **2017**, *315*, 10–17. [CrossRef]
13. Liu, E.; Long, M.; Zeng, J.; Luo, W.; Wang, Y.; Pan, Y.; Zhou, W.; Wang, B.; Hu, W.; Ni, Z. High Responsivity Phototransistors Based on Few-Layer ReS_2 for Weak Signal Detection. *Adv. Funct. Mater.* **2016**, *26*, 1938–1944. [CrossRef]
14. Hafeez, M.; Gan, L.; Li, H.; Ma, Y.; Zhai, T. Large-Area Bilayer ReS_2 Film/Multilayer ReS_2 Flakes Synthesized by Chemical Vapor Deposition for High Performance Photodetectors. *Adv. Funct. Mater.* **2016**, *26*, 4551–4560. [CrossRef]
15. Zhang, Q.; Wang, W.; Kong, X.; Mendes, R.G.; Fang, L.; Xue, Y.; Xiao, Y.; Rümmeli, M.H.; Chen, S.; Fu, L. Edge-to-edge oriented self-assembly of ReS_2nanoflakes. *J. Am. Chem. Soc.* **2016**, *138*, 11101–11104. [CrossRef] [PubMed]
16. Rahman, M.; Davey, K.; Qiao, S.Z. Advent of 2D Rhenium Disulfide (ReS_2): Fundamentals to Applications. *Adv. Funct. Mater.* **2017**, *27*, 1–29. [CrossRef]
17. Keyshar, K.; Gong, Y.; Ye, G.; Brunetto, G.; Zhou, W.; Cole, D.P.; Hackenberg, K.; He, Y.; Machado, L.; Kabbani, M. Chemical vapor deposition of monolayer rhenium disulfide (ReS_2). *Adv. Mater.* **2015**, *27*, 4640–4648. [CrossRef] [PubMed]
18. Al-Dulaimi, N.; Lewis, D.J.; Zhong, X.L.; Malik, M.A.; O'Brien, P. Chemical vapour deposition of rhenium disulfide and rhenium-doped molybdenum disulfide thin films using single-source precursors. *J. Mater. Chem. C.* **2016**, *4*, 2312–2318. [CrossRef]
19. Qi, F.; Chen, Y.; Zheng, B.; Zhou, J.; Wang, X.; Li, P.; Zhang, W. Facile growth of large-area and high-quality few-layer ReS_2 by physical vapour deposition. *Mater. Lett.* **2016**, *184*, 324–327. [CrossRef]
20. Chaturvedi, A.; Slabon, A.; Hu, P.; Feng, S.; Zhang, K.; Prabhakar, R.R.; Kloc, C. Rapid synthesis of transition metal dichalcogenide few-layer thin crystals by the microwave-induced-plasma assisted method. *J. Cryst. Growth* **2016**, *450*, 140–147. [CrossRef]
21. Afanasiev, P. Synthetic approaches to the molybdenum sulfide materials. *C. R. Chim.* **2008**, *11*, 159–182. [CrossRef]
22. Tang, G.; Sun, J.; Wei, C.; Wu, K.; Ji, X.; Liu, S.; Tang, H.; Li, C. Synthesis and characterization of flowerlike MoS_2 nanostructures through CTAB-assisted hydrothermal process. *Mater. Lett.* **2012**, *86*, 9–12. [CrossRef]
23. Li, N.; Chai, Y.; Li, Y.; Tang, Z.; Dong, B.; Liu, Y.; Liu, C. Ionic liquid assisted hydrothermal synthesis of hollow vesicle-like MoS_2 microspheres. *Mater. Lett.* **2012**, *66*, 236–238. [CrossRef]

24. Xie, J.; Zhang, H.; Li, S.; Wang, R.; Sun, X.; Zhou, M.; Zhou, J.; Lou, X.W.D.; Xie, Y. Defect-rich MoS_2 ultrathin nanosheets with additional active edge sites for enhanced electrocatalytic hydrogen evolution. *Adv. Mater.* **2013**, *25*, 5807–5813. [CrossRef] [PubMed]
25. Aliaga, J.A.; Alonso-Núñez, G.; Zepeda, T.; Araya, J.F.; Rubio, P.F.; Bedolla-Valdez, Z.; Paraguay-Delgado, F.; Farías, M.; Fuentes, S.; González, G. Synthesis of highly destacked ReS_2 layers embedded in amorphous carbon from a metal-organic precursor. *J. Non-Cryst. Solids* **2016**, *447*, 29–34. [CrossRef]
26. Tao, H.; Yanagisawa, K.; Zhang, C.; Ueda, T.; Onda, A.; Li, N.; Shou, T.; Kamiya, S.; Tao, J. Synthesis and growth mechanism of monodispersed MoS_2 sheets/carbon microspheres. *CrystEngComm* **2012**, *14*, 3027–3032. [CrossRef]
27. Cheng, L.; Huang, W.; Gong, Q.; Liu, C.; Liu, Z.; Li, Y.; Dai, H. Ultrathin WS_2 nanoflakes as a high-performance electrocatalyst for the hydrogen evolution reaction. *Angew. Chem. Int. Ed.* **2014**, *53*, 7860–7863. [CrossRef] [PubMed]
28. Kang, J.; Sangwan, V.K.; Wood, J.D.; Liu, X.; Balla, I.; Lam, D.; Hersam, M.C. Layer-by-Layer Sorting of Rhenium Disulfide via High-Density Isopycnic Density Gradient Ultracentrifugation. *Nano Lett.* **2016**, *16*, 7216–7223. [CrossRef] [PubMed]
29. Alonso, G.; Del Valle, M.; Cruz, J.; Petranovskii, V.; Licea-Claverie, A.; Fuentes, S. Preparation of MoS_2 catalysts by in situ decomposition of tetraalkylammoniumthiomolybdates. *Catal. Today* **1998**, *43*, 117–122. [CrossRef]
30. Alonso, G.; Berhault, G.; Paraguay, F.; Rivera, E.; Fuentes, S.; Chianelli, R.R. Mesoporous carbon-containing MoS_2 materials formed from the in situ decomposition of tetraalkylammoniumthiomolybdates. *Mater. Res. Bull.* **2003**, *38*, 1045–1055. [CrossRef]
31. Lu, X.; Lin, Y.; Dong, H.; Dai, W.; Chen, X.; Qu, X.; Zhang, X. One-step hydrothermal fabrication of three-dimensional MoS_2 nanoflower using polypyrrole as template for efficient hydrogen evolution reaction. *Sci. Rep.* **2017**, *7*. [CrossRef] [PubMed]
32. Devers, E.; Afanasiev, P.; Jouguet, B.; Vrinat, M. Hydrothermal syntheses and catalytic properties of dispersed molybdenum sulfides. *Catal. Lett.* **2002**, *82*, 13–17. [CrossRef]
33. Jacobsen, C.J.; Törnqvist, E.; Topsøe, H. HDS, HDN and HYD activities and temperature-programmed reduction of unsupported transition metal sulfides. *Catal. Lett.* **1999**, *63*, 179–183. [CrossRef]
34. Romero-Rivera, R.; Berhault, G.; Alonso-Nunez, G.; Del Valle, M.; Paraguay-Delgado, F.; Fuentes, S.; Salazar, S.; Aguilar, A.; Cruz-Reyes, J. Tungsten disulfide catalysts from tetraalkylammoniumthiotungstates by ex situ activation, their properties and HDS activity. *Appl. Catal. A* **2012**, *433*, 115–121. [CrossRef]
35. Davis, S. Photoemission studies of rhenium disulfide oxidation: Altered core-level structure and reactivity of defect sites. *Catal. Lett.* **1989**, *2*, 1–7. [CrossRef]
36. Daage, M.; Chianelli, R. Structure-function relations in molybdenum sulfide catalysts: The "rim-edge" model. *J. Catal.* **1994**, *149*, 414–427. [CrossRef]